

# Experimental observation of spectral oscillations in frequency modulation laser operation

Stefano Longhi

*Istituto Nazionale di Fisica per la Materia, Dipartimento di Fisica and CEQSE-CNR, Politecnico di Milano, Piazza Leonardo da Vinci 32, I-20133 Milano, Italy*

(Received 4 May 2001; published 24 September 2001)

The experimental observation of transient coherent oscillations in the optical frequency spectrum of an Er–Yb solid-state laser with internal frequency modulation (FM) is reported. These oscillations, which arise in the presence of a slight detuning between the modulation frequency and the cavity axial mode separation, are transiently observed when the modulator is switched on and appear as a damped breathing of laser spectral width superimposed to the relaxation oscillation dynamics of the laser intensity. The experimental results are in good agreement with the theoretical predictions which take into account both the fast dynamics of spectral oscillations and the slow dynamics of relaxation oscillations for the codoped Er–Yb laser system.

DOI: 10.1103/PhysRevE.64.047201

PACS number(s): 05.45.–a, 42.60.Fc, 42.60.Mi

The study of the dynamical behavior hidden in intracavity frequency modulation (FM) of a laser [1,2] has received in recent years a renewed interest [3–5], mainly motivated by the potential applications of FM-operated lasers for the generation of highly coherent optical signals and ultrashort laser pulses [6–9]. The modulation of the optical cavity length of a laser at a frequency  $\nu_m$  close to the cavity axial mode separation  $\nu_{ax}$  or to an integer multiple  $N\nu_{ax}$  (harmonic regime) is known to lead to the generation of a mode locked pulse train (FM mode locking) under synchronous modulation ( $\nu_m = N\nu_{ax}$ ), or to the generation of a frequency-modulated optical field (FM laser oscillation) for a detuned modulation [1,2]. In the latter case the output laser field may be described approximately as a frequency-modulated signal with an effective modulation index strongly enhanced by a cavity effect and given by  $\Gamma = \Delta/(2\pi\gamma)$ , where  $\Delta$  is the modulation depth impressed by the modulator in one cavity round-trip and  $\gamma = N(N\nu_{ax} - \nu_m)/(\nu_m)$  is the normalized frequency detuning parameter ( $N=1$  if the laser is operated in the fundamental harmonic regime) [1,2]. Despite this simple picture, FM laser oscillation hides a variety of intriguing dynamical aspects. From the experimental side, FM lasers suffer from amplitude noise at frequency detuning and harmonics, which is undesirable in applications [9]. It was pointed out that this noise may be of both dynamical as well as of stochastic origin [4,5]. In Ref. [4] it was shown that internally FM lasers have some form of excess noise similar to that found in detuned amplitude-modulated mode-locked lasers [10], which is especially large when approaching the transition from the FM regime to the pulsed FM mode locking. In Ref. [5] further insights into dynamical aspects underlying low-frequency noise in FM lasers were added. In particular, the existence of coherent oscillations of the spectral width of the field emitted by an FM-operated laser (“spectral oscillations”) was theoretically predicted, and in the reversible case a simple mechanical analogy of the breathing spectral dynamics was pointed out. Such coherent oscillations play an important role in the transient dynamics leading to the formation of the FM laser spectrum from single longitudinal mode laser emission when the modulator is switched on. In the simplest case of a laser cavity with infinite gain bandwidth, the field dynamics is reversible, i.e., any

initial spectral field distribution is periodically recovered with a period  $\delta T = 1/(\gamma\nu_{ax})$ , and spectral oscillations are undamped. In particular, if the modulator is switched on at time  $t=0$  and the laser oscillates on a single longitudinal mode, the laser spectrum shows a reversible breathing dynamics with Bessel sideband modes corresponding to a modulation index  $\Phi$  that varies periodically in time between  $\Phi=0$  and  $\Phi=2\Gamma$  according to  $\Phi(T) = \Gamma\sqrt{2-2\cos(2\pi\gamma T)}$ , where  $T = t/T_R$  is the round-trip number and  $T_R = 1/\nu_{ax} \approx N/\nu_m$  is the cavity round-trip time (see Fig. 1). If finite gain bandwidth effects of the cavity are considered, the reversible dynamics is broken and spectral oscillations are damped out with a final steady-state spectral mode corresponding to the modulation index  $\Gamma$ ; in addition, in case of solid-state lasers with a slow gain dynamics, relaxation oscillations are transiently excited owing to an excess gain that is needed to support the FM mode [5].

In this work, the experimental observation of transient oscillations of the spectral width of an FM-operated Er–Yb laser during buildup of the FM spectrum from single-longitudinal mode operation is reported. This analysis represents what it is believed to be the first experimental study of the transient dynamics leading to the formation of the FM spectrum in an internally modulated laser. The experimental

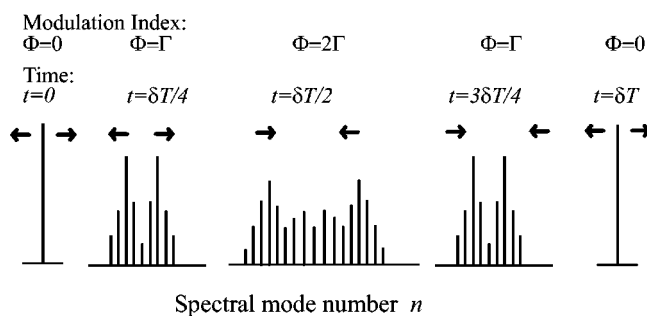


FIG. 1. Schematic of the breathing dynamics of the spectrum of an FM laser after switch on of the modulator in the case of an infinite gainline. The modulation index of the FM spectrum varies periodically between zero, corresponding to a single mode attained at times  $t=0$ ,  $t=\delta T$ ,  $t=2\delta T$ ,  $\dots$ , and  $2\Gamma$ , attained at times  $t=\delta T/2$ ,  $t=3\delta T/2$ ,  $t=5\delta T/2$ ,  $\dots$ , where  $\delta T = T_R/\gamma$ .

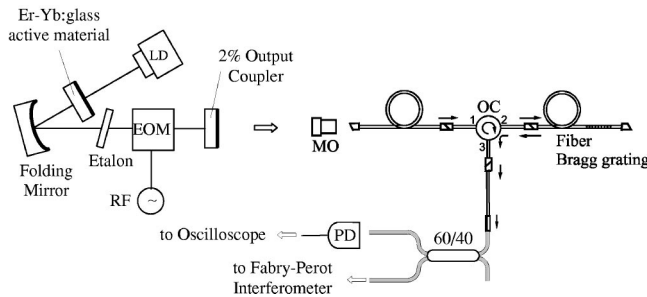


FIG. 2. Experimental layout for the study of transient dynamics of the FM-operated Er–Yb laser. LD: laser diode; EOM: electro-optic phase modulator; MO: microscope objective; OC: optical circulator; PD: photodiode; and RF: radio-frequency synthesizer.

setup is shown in Fig. 2. The laser source, similar to that described in Refs. [7,9], is a 18-cm-long one-folded Er–Yb:glass laser frequency modulated by an intracavity LiNbO<sub>3</sub> phase modulator driven at 2.49 GHz by a radio-frequency (rf) synthesizer in a third-harmonic configuration ( $N=3$ ). The active medium is a 1-mm-thick QX20 phosphate glass disk, doped with erbium and codoped with ytterbium, end-pumped at 980 nm by an InGaAs laser diode. An intracavity 100- $\mu$ m-thick uncoated BK7 etalon reduces the gain bandwidth of the cavity and allows for single longitudinal mode operation, when the modulator is switched off, at a wavelength tunable by a few nanometers around 1533 nm. The laser output is launched into an optical fiber and both laser intensity and laser spectrum are simultaneously detected with a low-noise photodiode (New Focus model 1811, 125 MHz electrical bandwidth) and a scanning Fabry–Perot interferometer (Burleigh Mod. IR-110) with a free-spectral range of 150 GHz and a finesse of  $\sim 90$ . When the modulator is switched on, under proper tuning of cavity length a typical FM spectrum with Bessel sideband modes is observed after transient, with a spectral extent that depends on cavity length tuning. A precise control of frequency detuning  $\delta\nu = N\nu_{ax} - \nu_m$  is accomplished by changing the driving modulation frequency from exact synchronism, which is attained when the laser is FM mode locked. I typically set the frequency detuning  $\delta\nu$  at 2.9 MHz and the rf power level such that  $\Delta \sim 0.29$ , corresponding to an effective modulation index  $\Gamma \sim 13$ . The laser is operated at a pump power about four times above its threshold value, and in this condition an output power of  $\sim 8$  mW is available for the experiment. The spectrum of the FM laser after transient, as measured by the Fabry–Perot interferometer, is shown in Fig. 3(a). The measured switch-on time of the rf sinusoidal wave form that drives the modulator is  $\sim 5 \mu\text{s}$ , and it may be considered as instantaneous for our purposes. The transient of laser intensity during switch on of the modulator, shown in Fig. 3(b), indicates the appearance of damped relaxation oscillations at a frequency  $\nu_{\text{relax}} \sim 65$  kHz, however, the slow response of the Fabry–Perot interferometer is not able to detect the transient dynamics of the spectral laser output, and hence the occurrence of spectral oscillations. In order to get some insights into the spectral dynamics, a spectral filtering of the laser field was achieved using a fiber Bragg grating in a configuration similar to that adopted in Ref. [7] to generate

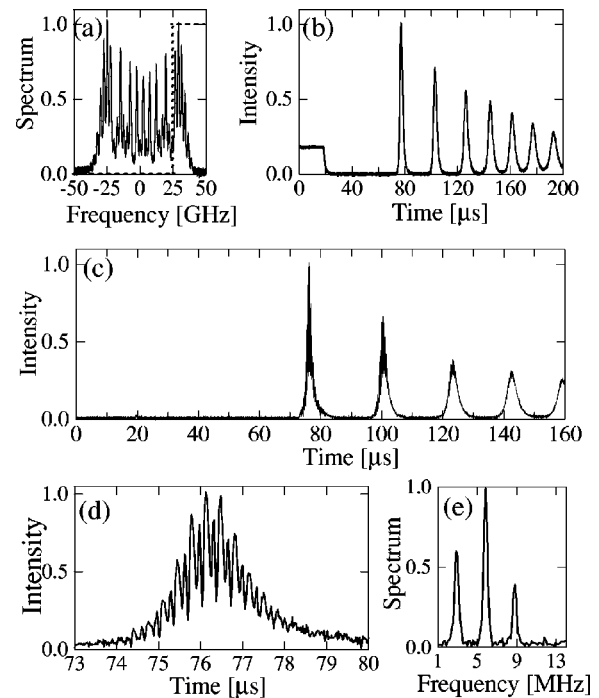


FIG. 3. Transient dynamics of the FM-operated Er–Yb laser after switching on the phase modulator. (a) Laser spectrum after initial transient; (b) intensity of total laser field, showing relaxation oscillation dynamics in the tens of microseconds time scale; (c) intensity of the spectrally filtered laser field; (d) enlargement of the first relaxation oscillation pulse of (c), showing internal oscillations in the submicrosecond time scale; and (e) numerically computed spectrum of the wave form of (d). Arbitrary units are used to represent both intensity and spectrum curves. The dashed curve in (a) is the spectral power reflectivity of the fiber grating used for spectral filtering. The breathing dynamics of the FM spectrum during transient is transformed into an oscillation of the field intensity reflected by the grating.

transform-limited pulse trains from a FM signal. The fiber grating, designed to operate in the reflection configuration as an almost ideal step filter, is used to filter the anti-Stokes part of the spectral content of the laser field at steady state [see Fig. 3(a)]. Oscillations of the spectral extent of the laser field during transient are hence converted into oscillations of the intensity of the filtered signal reflected by the grating, which is retrieved by the use of an optical circulator as indicated in Fig. 2. A typical transient behavior of the intensity of the filtered signal is shown in Fig. 3(c). In this case, besides the occurrence of relaxation oscillations in the tens of microseconds time scale, damped oscillations in the submicrosecond time scale are clearly visible, as shown in Fig. 3(d). The numerically computed spectrum of the signal of Fig. 3(d), shown in Fig. 3(e), indicates that the fast oscillations inside the long relaxation oscillation pulse occur exactly at the detuning frequency and harmonics, which is a signature of the spectral breathing dynamics predicted in Ref. [5].

To get a deeper understanding of the experimental results I have theoretically simulated the transient dynamics of the Er–Yb FM laser and compared the theoretical predictions with the experimental data. The model of the FM-operated

laser is basically that previously considered in Ref. [5], extended to allow for harmonic FM operation and to properly account for the gain dynamics of the codoped Er–Yb system [11]. After introduction of the expansion  $E(t) = \sum_n F_n(t) \exp(2\pi i n \nu_m t)$  for the electric field  $E(t)$ , the slow evolution of the amplitudes  $F_n$  reads [4,5]

$$\frac{dF_n}{dT} = \left[ -2\pi i \gamma n + \frac{g}{2} - \frac{l}{2} - n^2 \left( \frac{\nu_m}{\nu_g} \right)^2 \right] F_n + i \frac{\Delta}{2} (F_{n+1} + F_{n-1}), \quad (1)$$

where  $T = t/T_R$  is the round-trip number,  $T_R \approx N/\nu_m$  is the round-trip time,  $\gamma = N(N\nu_{ax} - \nu_m)/\nu_m$  is the normalized frequency detuning parameter ( $|\gamma| \ll 1$ ),  $\nu_g$  is the spectral bandwidth of the gainline,  $g$  and  $l$  are round-trip saturated gain and cavity loss rate in intensity, respectively, and  $\Delta$  is the round-trip modulation index introduced by the phase modulator. To account for the dynamics of the gain  $g$  we need to consider the rate equations of both erbium and ytterbium populations on ground state ( $^4I_{15/2}$  for  $\text{Er}^{3+}$  and  $^2F_{7/2}$  for  $\text{Yb}^{3+}$ ) and on upper state ( $^4I_{13/2}$  for  $\text{Er}^{3+}$  and  $^2F_{5/2}$  for  $\text{Yb}^{3+}$ ). In fact, in the codoped Er–Yb system population inversion is achieved by an effective energy transfer mechanism of excitation of optically inverted Yb ions to Er ions. A rate-equation modeling of the Er–Yb laser system, which includes the energy transfer and other dissipative processes, is discussed in detail in Ref. [11]. After introduction of the round-trip gain coefficients  $g = 2\sigma_{\text{Er}}\Delta N_{\text{Er}}L$  and  $G = 2\sigma_{\text{Yb}}\Delta N_{\text{Yb}}L$  for  $\text{Er}^{3+}$  and  $\text{Yb}^{3+}$  transitions, where  $\sigma_{\text{Er},\text{Yb}}$  and  $\Delta N_{\text{Er},\text{Yb}}$  are cross sections and population inversions of the transitions, respectively, and  $L$  is the thickness of the active medium, the rate equations for  $g$  and  $G$  can be cast in the following form:

$$\frac{dg}{dT} = -(T_R/\tau_{\text{Er}})[g + g_0 + g\mathcal{E} + \alpha(G + G_0)(g - g_0) + \rho(g + g_0)^2], \quad (2a)$$

$$\frac{dG}{dT} = -(T_R/\tau_{\text{Yb}})[G + G_0 + \tau_{\text{Yb}}W(G - G_0) + \beta(G + G_0)(g_0 - g)], \quad (2b)$$

where  $\tau_{\text{Er}}$  and  $\tau_{\text{Yb}}$  are the fluorescence lifetimes of  $\text{Er}^{3+}$  and  $\text{Yb}^{3+}$  upper levels,  $g_0 = 2\sigma_{\text{Er}}N_{\text{Er}}L$  and  $G_0 = 2\sigma_{\text{Yb}}N_{\text{Yb}}L$  are the round-trip absorption coefficients of  $\text{Er}^{3+}$  and  $\text{Yb}^{3+}$  transitions in the absence of pumping,  $N_{\text{Er}}$  and  $N_{\text{Yb}}$  are the populations of Er and Yb ions in the host glass,  $W$  is the pump rate of Yb ions in the upper pump level,  $\alpha = k\tau_{\text{Er}}/(4\sigma_{\text{Yb}}L)$  and  $\beta = k\tau_{\text{Yb}}/(4\sigma_{\text{Er}}L)$  are dimensionless parameters that account for the energy transfer process from Yb to Er ions,  $k$  is the rate of energy transfer,  $\rho = C\tau_{\text{Er}}/(4\sigma_{\text{Er}}L)$  is a dimensionless parameter that accounts for up conversion of Er ions,  $C$  is the rate of up-conversion process, and  $\mathcal{E} = \sum_n |F_n|^2$  is the

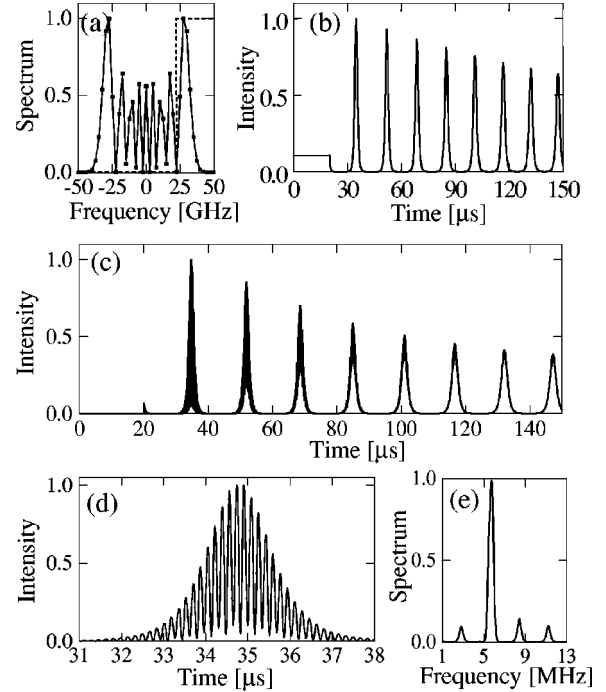


FIG. 4. Same as Fig. 3, but from numerical simulations of Eqs. (1) and (2). The parameter values used in the simulation are  $\Delta = 0.29$ ,  $\gamma = 0.0035$ ,  $l = 0.06$ ,  $\nu_g/\nu_m = 316$ ,  $L = 1$  mm,  $N_{\text{Er}} = 2 \times 10^{20}$  cm $^{-3}$ ,  $\tau_{\text{Er}} = 8$  ms,  $\sigma_{\text{Er}} = 8 \times 10^{-21}$  cm $^2$ ,  $N_{\text{Yb}} = 2 \times 10^{21}$  cm $^{-3}$ ,  $\tau_{\text{Yb}} = 1.1$  ms,  $\sigma_{\text{Yb}} = 7 \times 10^{-21}$  cm $^2$ ,  $k = 2 \times 10^{-16}$  cm $^3$ /s, and  $C = 1 \times 10^{-18}$  cm $^3$ /s. A pump rate  $W$  four times above its threshold value has been assumed in the simulation, and 61 spectral modes have been considered in Eq. (1).

normalized energy of the field in one cavity round-trip time. The coupled equations (1) and (2) have been numerically integrated using a fourth-order variable-step Runge–Kutta method, and the results of the numerical simulations are summarized in Fig. 4. The parameter values used in the simulations are given in the caption of Fig. 4; the laser parameters entering in Eq. (1), e.g., loss rate  $l$ , gain bandwidth  $\nu_g$ , modulation depth  $\Delta$ , and detuning  $\gamma$ , are taken in compliance with the experiment, whereas the material parameters entering in Eq. (2) have been taken from Ref. [11]. As an initial condition we assumed the steady-state solution corresponding to the single-longitudinal mode emission which is obtained from Eqs. (1) and (2) by assuming  $F_n = 0$  for  $n \neq 0$ ,  $\Delta = 0$  and setting equal to zero the time derivatives. The agreement between the experimental results of Fig. 3 and the theoretical simulations of Fig. 4 is rather satisfactory, including the appearance of high-harmonic components in the spectral oscillations. The anharmonic terms in the breathing spectral dynamics observed both in the experiment and in the simulations [see Figs. 3(e) and 4(e)] are due to the finite gain bandwidth of the laser, which introduces a complex interference of Floquet modes of the phase-modulated cavity during the decay process of spectral oscillations [5]. A disagreement between theory and experiment is the time delay for the appearance of the first relaxation oscillation peak after the modulation is switched off, which is considerably longer in

the experiment [compare Figs. 3(b) and 4(b)]. A possible explanation thereof is that in the theoretical model the relaxation oscillation dynamics is triggered solely by the excess gain needed to support the FM mode as compared to the single longitudinal mode of the not-modulated laser [5]; in the experiment, a transient misalignment of the laser resonator introduced by modulator beam deflection may act as an additional source of gain imbalance that makes longer the transient built-up time of laser intensity after the modulator is switched on.

In conclusion I have experimentally investigated for the first time the transient dynamics of an internally frequency-modulated Er–Yb solid-state laser and revealed the existence of damped spectral oscillations in the detuned mode of operation, which is a signature of the spectral breathing dynamics previously predicted in Ref. [5]. The present analysis adds further insights into the hidden dynamical behaviors of FM operated lasers and may be helpful to explain the low-frequency amplitude noise observed in these types of lasers [9].

- 
- [1] S.E. Harris and O.P. McDuff, *Appl. Phys. Lett.* **5**, 205 (1965); *IEEE J. Quantum Electron.* **QE-1**, 245 (1965); A. Yariv, *J. Appl. Phys.* **36**, 388 (1965).
- [2] A.E. Siegman, *Lasers* (University Science Books, Mill Valley, CA, 1986), Sect. 27.7, pp. 1095–1101.
- [3] S. Longhi and P. Laporta, *Appl. Phys. Lett.* **73**, 720 (1998); *Phys. Rev. A* **60**, 4016 (1999).
- [4] S. Longhi and P. Laporta, *Phys. Rev. E* **61**, R989 (2000).
- [5] S. Longhi, *Phys. Rev. E* **63**, 037201 (2001).
- [6] A. Schremer, T. Fujita, C.F. Lin, and C.L. Tang, *Appl. Phys. Lett.* **52**, 263 (1988); A. Schremer and C.L. Tang, *ibid.* **55**, 1832 (1989).
- [7] S. Longhi, S. Taccheo, and P. Laporta, *Opt. Lett.* **22**, 1642 (1997); S. Longhi, G. Sorbello, S. Taccheo, and P. Laporta, *ibid.* **23**, 1547 (1998).
- [8] K.S. Abedin, N. Onodera, and M. Hyodo, *Electron. Lett.* **34**, 1321 (1998); *Opt. Commun.* **158**, 77 (1998); *Jpn. J. Appl. Phys., Part 2* **37**, L1046 (1998); *Opt. Lett.* **24**, 1564 (1999).
- [9] S. Longhi, M. Marano, P. Laporta, O. Svelto, R. Corsini, and F. Fontana, *Appl. Phys. B: Lasers Opt.* **B69**, 487 (1999); M. Marano, S. Longhi, and P. Laporta, *Electron. Lett.* **35**, 1877 (1999); M. Marano, S. Longhi, G. Sorbello, P. Laporta, M. Pulseo, and P. Gambini, *ibid.* **36**, 1287 (2000).
- [10] H.J. Eichler, I.G. Koltchanov, and B. Liu, *Appl. Phys. B: Lasers Opt.* **B61**, 81 (1995); F.X. Kärtner, D.M. Zumbühl, and N. Matuschek, *Phys. Rev. Lett.* **82**, 4428 (1999).
- [11] P. Laporta, S. Taccheo, S. Longhi, O. Svelto, and C. Svelto, *Opt. Mater.* **11**, 269 (1999).